MAGNETIC PHASE TRANSITIONS IN Gd-RICH METALLIC GLASSES

by

JAAFAR JANTAN

B.Sc., Kansas State University, 1983

A MASTER'S THESIS

submitted in partial fulfillment of the

requirements for the degree

MASTER OF SCIENCE

Department of Physics

Kansas State University

Manhattan, Kansas

1985

Approved by:

Michael J. Sabo

Major Professor

TABLE OF CONTENTS

LIST OF FIGURES

LIST OF TABLES

ACKNOWLEDGEMENTS

I would like to thank the Almighty God.

I would like to thank my family for their love and encouragement over the years.

I would like to thank my wife for her love and understanding and to my daughter Nita Azlin.

I would like to thank Dr. M.J. O'Shea for his guidance, help and patience throughout the duration of my study.

I would like to thank all the faculty members in this department for their encouragement.

I wish to thank Zurah and Sadiah for their help in labelling figures.

I would like to acknowledge my Malaysian friends and Muslim brothers for their friendship.

I acknowledge the Ministry of Education and the Malaysian Government for sponsoring my studies.

I thank Dr. G.C. Hadjipanayis for his generosity in providing us with liquid Helium and letting us use some of his apparatus.

I thank Dr. D.J. Sellmeyer at the University of Nebraska at Lincoln for the use of the splat-cooling apparatus.

A word of thanks to Janie Torrey for typing this thesis.

Finally, I acknowledge the Research Coporation for its financial support.

Chapter 1

INTRODUCTION

Study of magnetism in amorphous systems began in 1960 when Gubanov[1] discovered that lattice periodicity is not an essential requirement for ferromagnetism(FM). Amorphous or glassy structure refers to the absence of long-range structural lattice periodicity, Crystallinity, on the other hand, refers to a solid with long-range periodicity.

For the past decade, work on metallic glasses[2] has been of great interest. Metallic glasss were first prepared successfully by Duwez et al.[3] by rapidly quenching the alloy. Various methods of rapid quenching include melt-spining, splat cooling and the evaporation technique.

The discovery of a transition from a paramagnetic (PM) state to a spin-glass (SG)[4-5] state where spins are frozen in random directions has led to extensive study of amorphous magnetic systems. More recently, double transition behavior has been found in similar systems. Here, a ferromagnetic (FM) state is present at intermediate temperatures before the low temperature SG state is entered. The SG state is similar to the PM state in that the spins are randomly oriented with zero net magnetization. However, spins are frozen in the SG state and non-equilibrium behavior (such as hysteresis and long time-dependent magnetization) is also present.

It was believed that spin glasses could be treated as if they have a true equilibrium phase transition.[6-8] Computer simulations using the Monte Carlo[9] technique and models of spin glasses by a number of authors[10-11] suggest that the SG phase transition is a true equilib-

rium phase transition. The solution to the Sherrington-Kirkpatrick (SK)[10] model indicates double transition behavior may exist in metallic glasses. Even though this model applies only for lattice dimensionality d>4, the solution mimics a number of experimental observations.

Computer simulations of systems with short-range interactions, however, fail to produce any double transition behavior. These can however produce a PM-SG transition. Frustration in microscopic interactions including anisotropic interactions seem to be the only criteria for a SG transition in these simulations. Existence of the SG state in double transition systems suggest that anisotropy[12] is present in these systems also.

Experimental observations on amorphous Fe-Mn[13-15], Fe-Ni[16] and Gd-La[17-18] systems reveal double transition behavior similar to that of the SK model. The static scaling hypothesis has been used to analyse data near the FM-SG transition. Low field measurements done by Manheimer et al.[13] on the Fe-Mn systems and scaling analyses done by several others[14-18] imply that the FM-SG transition is a true equilibrium phase transition.

This work concentrates on $Gd_xTM_{72-x}G_{28}$ systems where TM = Mn, Ni, La and $G_{28} = Ga_{18}B_{10}$. The Gd-La system is studied to compare it to previous work. We shall study the PM-FM and FM-SG transition in detail by measuring the susceptibility and magnetization in low fields. A static scaling analysis will be used to examine behavior near these transitions. In addition, non-equilibrium behavior is also investigated.

Chapter 2

THEORETICAL ASPECTS

2.1 Magnetism of rare-earth and transition metals.

The rare-earths[19] are the fifteen elements from La(Z = 57) to Lu(Z = 71). For isolated rare-earth atoms, the normal electronic configuration is $(Pd)^{46}\ 4f^n\ 5s^2 5p^6 5d^1 6S^2$ where n is the number of electrons in the 4f shell. The magnetic moment of rare-earth ions arises from a partial filling of the 4f shell. This shell is well localized and there is, therefore, negligible overlap between 4f wavefunctions centered on neighboring atoms. In the metallic state the 5d and 6s valence electrons are delocalized and form a conduction band.

The magnetism of the rare-earths can be attributed to the localized moments of the 4f shell. Spins in the unfilled 4f shell are arranged according to Hund's rules.[20] For the Gd^{3+} ion, there are 7 electrons in the 4f shell. Following Hund's rules, all the spins are arranged parallel to each other exactly half-filling the shell. Thus, the angular momentum $|\vec{S}| = 7/2$, $|\vec{L}| = 0$ and so $|\vec{J}| = |\vec{S}| = 7/2$. Since $|\vec{L}| = 0$ for the Gd^{3+} ion, the charge distribution is spherically symmetric. In all other magnetic rare-earths, the angular momentum $|\vec{L}|$ is non-zero leading to a non-spherical charge distribution and large random electric field gradients. For La^{3+}, all the shells are completely filled and therefore both L and S are zero resulting in a zero net moment.

For the 3d transition metals, the normal electronic configuration for isolated atoms is $(A)^{18} 3d^n 4s^2$ where n is the number of electrons in the 3d shell. The 3d moments in transition metals are not isolated

and the wavefunctions centered on neighboring atoms overlap. On alloying, the 3d levels may be considerably modified. In the crystalline state, moments on different sites have the same value whereas in an amorphous state moments have a distribution of values for a given alloy and depend on the local electronic environment. As a result, values of the moment change on going from the crystalline to amorphous state.

In most transition metals, the direct exchange interaction is the dominant interaction betweem moments. Magnetic electrons of the 3d shells are partially localized. One atom interacts with its neighbors via direct exchange. This exchange is strong in transition-metal-rich alloys. Exchange between moments in elemental Ni and Fe is ferromagnetic whereas in Cr and Mn, the exchange is antiferromagnetic.

In the rare-earths, direct exchange does not play an important role. Since 4f magnetic electrons are well shielded, they are highly localized. In this case, the RKKY (Ruddermann, Kittel, Kasuya, Yosida)[21-24] exchange interaction is responsible for magnetic ordering. This is an indirect exchange and information is mediated by conduction electrons. In Fig. 1a, the exchange interaction J_{ij} is plotted as a function of atomic separation r_{ij} and it oscillates from ferromagnetic to antiferromagnetic for different atomic sites. This oscillation is a result of screening of magnetic ions by conduction electrons. As a result, a magnetic ion can receive contradictory exchange information from its neighbors leading to frustration. In crystals, the oscillation envelope varies as $1/r^3$ whereas in metallic glasses, it is believed to fall off somewhat faster.

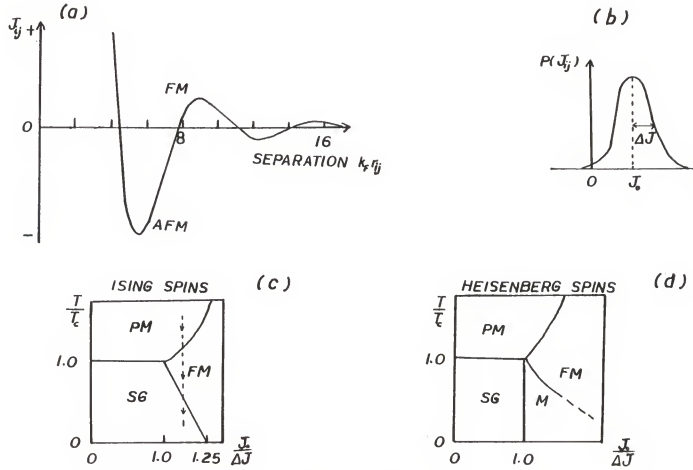

Figure 1: (a) Dependence of the RKKY exchange interaction on distance. (b) Probability distribution for J_{ij}. (c) Magnetic phase diagram calculated by Sherrington and Kirkpatrick using Ising spins. (d) Magnetic phase diagram calculated using Heisenberg spins(see text for definition of symbols used).

2.2 Phase Transitions and Critical Behavior

A. Phase Transitions and the Mean Field Theory of Ferromagnetism

Phase transition[6-8] in a magnetic system are characterized by a change in an order parameter M, the magnetization. In the paramagnetic state, M is zero. As the temperature is lowered below the PM-FM transition temperature a FM transition occurs and M becomes non-zero. This phase transition is a continuous phase transition. More accurately, it is a second order phase transition.[9,26] The isothermal susceptibility

$$\chi_T = \left(\frac{\partial M}{\partial H}\right)_T$$

diverges for $T \to T_{pf}^{+}$ characteristic of a second order phase transition. In addition, M increases continuously below T_{pf} indicative of a second order phase transition. The PM-FM transition in metallic glasses is generally accepted to be a true phase transition.

According to mean field theory,[8,20] below a temperature T_{pf}, spins interact through a molecular field proportional to the average magnetization. This field arises from the Heisenberg exchange interaction between spins. The Hamiltonian for a system of N non-interacting spins in an external field $\vec{H}$ can be written as

$$\mathcal{H}_{NI} = g\mu_B \sum_{i=1}^{N} \vec{S}_i \cdot \vec{H}$$

where g is the Lande factor and μ_B is a Bohr magneton.

Mean field theory in crystalline systems assume that interactions between spins may be modelled by an effective field $\vec{H}_m$ ($\vec{B} = \mu\vec{H}_m = \lambda\vec{M}$) giving a Hamiltonian

$$\mathcal{H}_{MF} = g\mu_B \sum_{i=1}^{N} \vec{S}_i \cdot (\vec{H}+\vec{H}_m)$$

Analysis of this Hamiltonian gives a PM-FM transition temperature

$$\mathcal{H}_{T_{pf}} = \lambda N (g\mu_B)^2 \, S(S+1)/3k_B$$

where λ is the molecular field constant and k_B a Boltzmann constant.

Within the framework of a Heisenberg model, the effective field in mean field theory comes from an exchange interaction between the magnetic moments $\vec{S}_i$ and $\vec{S}_j$ localized on sites i and j, which can be represented by

$$\mathcal{H}_H = - \sum_{i,j=1}^{N} J_{ij} \, \vec{S}_i \cdot \vec{S}_j$$

where J_{ij} is an exchange parameter. Positive J_{ij} favors parallel alignment of spins (ferromagnetic ordering) while negative J_{ij} favors anti-parallel alignment of spins (antiferromagnetic order). The mean field approximation to the Heisenberg model gives the PM-FM transition temperature

$$T_{pf} = \frac{2}{3k_B} \hat{J}_o \, S(S+1)$$

where $\hat{J}_o = qJ$ and q is the coordination number. This equation predicts that as long as the coordination number is the same, T_{pf} will have the same value independent of lattice dimensionality. This means that mean field theory is too crude to take into account lattice dimensionality which is known to be one of the crucial features determining critical behavior.

B. Critical Exponents and the Scaling Hypothesis

The critical exponents[8] are a set of indices used to describe functions or order parameters near a phase transition. In a lot of cases, critical exponents are used instead of the complete functional form because they are calculable for many models. Sufficiently near the critical region, behavior of the leading terms in the functional form dominates. Thus, log-log plots of experimental data yielding straight lines will give the critical indices by simply taking the slope of the lines. A list of critical exponent definitions is presented in Table 1a and values of the critical indices for mean field theory, the classical Heisenberg (d=3) model and a number of crystalline elements are presented in Table 1b.

Inequalities between the critical exponents may be drived from general thermodynamic arguments. These relations among critical exponents are satisfied as equalities according to the static scaling hypothesis.[8] This hypothesis asserts that the Gibbs potential in reduced form $G(\varepsilon,H)$, ($\varepsilon = (T-T_{pf}) / T_{pf}$) is a generalized homogeneous function and the equalities listed in Table 1c follow from this.

In addition, the scaling hypothesis also makes specific predictions concerning the form of the magnetic equation of state which are supported by experimental observations in crystalline insulating and metallic ferromagnetic systems. According to the static scaling hypothesis, the equation of state can be written as

$$m = m\left(\frac{\varepsilon}{|\varepsilon|}, h\right)$$

where $m = M(\varepsilon,H) / |\varepsilon|^{\beta}$ and $h = H(\varepsilon,M) / |\varepsilon|^{\beta\delta}$ are the reduced magnetization and reduced magnetic field respectively; β and δ are the

Table 1a: Summary of Definitions of the Static Critical Point Exponents for Magnetic Systems

Exponent	Definition	Conditions ε	H	M	Quantity	Ref.
α'	$C_H \sim (-\varepsilon)^{-\alpha'}$	<0	0	0	Specific heat at constant	8
α	$C_H \sim \varepsilon^{-\alpha}$	>0	0	0	magnetic field.	
β	$M \sim (-\varepsilon)^{\beta}$	<0	0	$\neq 0$	Zero field magnetization.	
γ'	$\chi_T \sim (-\varepsilon)^{-\gamma'}$	<0	0	$\neq 0$	Zero field isothermal	
γ	$\chi_T \sim \varepsilon^{-\gamma}$	>0	0	0	susceptibility.	
δ	$H = \lvert M \rvert^{\delta}$	0	$\neq 0$	$\neq 0$	Critical isotherm.	

Table 1b: Values of critical exponents for mean field and Heisenberg models and experimental values for a number of crystalline elements near the PM-FM transition.

System	β	δ	Ref.
Mean field	0.5	3.0	8
Heisenberg (d=3)	0.35	5.0	
Fe (crystal)	0.389	4.35	
Mi (crystal)	0.378	4.58	
Gd (crystal)	0.38	3.61	

Table 1c: Relations among the static critical exponents predicted by the scaling hypothesis. These relations are not all independent of one another and in fact knowledge of two exponents suffices to determine the remaining ones.

		Ref.
1.	$\alpha + 2\beta + \gamma = 2$	8
2.	$\alpha + \beta(\delta+1) = 2$	
3.	$\gamma(\delta+1) = (2-\alpha)(\delta-1)$	
4.	$\gamma = \beta(\delta-1)$	

critical indices related to M below T_{pf} and H at T_{pf} respectively. According to this equation, near a critical region, plots of m vs. h have only two branches; one above T_{pf} ($\varepsilon/|\varepsilon|=+1$) and the other below T_{pf}($\varepsilon/|\varepsilon|=-1$). On the other hand, plots of M vs. H for various temperatures fall on distinct isotherms.

This hypothesis will be applied for analysis of data near the FM-FM and FM-SG transitions. The FM-SG transition is of considerable interest since it is not yet clear whether this is a true phase tran sition.

2.3 Frustrated Systems

A. Mean Field Theory

The origin of the spin glass[4-5] state in Gd-rich alloys is attributed to the RKKY interaction in J_{ij}. At low temperatures, if there are sufficient antiferromagnetic interactions between moments, spins will feel frustration effects. Below the FM-SG transition temperature, frustrated spins are frozen in random orientations characteristic of a SG state.

In models, the general approach is to consider fluctations ΔJ in the exchange interaction J_{ij} about some positive mean value J_o (ferromagnetic). The exchange is often represented by a Gaussian distribution

$$P(J_{ij}) = \frac{1}{\sqrt{2\pi}\Delta J} \exp\left[-(J_{ij}-J_o)^2/2(\Delta J)^2\right]$$

as illustrated in Fig. 1b. Within the mean field model Handrich and Kobe[25-27] have shown that the effect of fluctuations is to lower the T_{pf} and reduce the magnetization. Within the same model, Sherrington-

Kirkpatrick (SK)[10] calculated transition temperatures as a function of $J_o/\Delta J$ using Ising spins. The Hamiltonian for this model is written as

$$\mathcal{H}_{SK} = - \sum_{ij} (J_o + \Delta J_{ij}) \vec{S}_i \cdot \vec{S}_j$$

A schematic of the SK model phase diagram is shown in Fig. 1c. For large fluctuations ($J_o/\Delta J < 1$) there is only a PM-SG transition whereas for small fluctuations ($J_o/\Delta J > 1$) there is double transition behavior namely a PM-FM transition at T_{pf} and a FM-SG transition at T_{fg}.

The SK solution to the above Hamiltonian mimics experimental results. Unfortunately, the calculation holds only for space dimensionality d>4. In addition, calculations and computer simulations (within mean field theory) using Heisenberg spins do not produce the double transition behavior. This may be seen from the calculated phase diagram of Fig. 1d. The dashed line in the figure represents the onset of non-equilibrium behavior with M being a mixed phase where FM and SG states coexist.

Computer simulations (of systems with short range interactions) require frustration in the microscopic interactions including a small anisotropic interaction in the case of Heisenberg spins, to produce the PM-SG transitions in metallic glasses. It is not known what microscopic interactions are required for double transitions but the existence of a SG phase with its non-equilibrium behavior suggests anisotropic interaction must be included.[12,17] Thus, one has to study the non-equilibrium behavior as well as the scaling behavior to gain more insight into the SG state.

B. Review of Previous Work

In the last five years SG and double transition behavior have been investigated in a number of systems. Yeshurun et al.[14] studied the Fe-Mn system and obtained a phase diagram similar to that of the SK model. Double transition behavior was observed in their investigations. In the absence of any theory to compare to near the FM-SG transition, the static scaling hypothesis was applied to study the scaling behavior. From the decrease in M below T_{fg} (FM-SG transition temperature) and the scaling of the initial magnetization obtained at this transition, they concluded that the FM-SG transition is a true phase transition.

The magnetic properties of the Fe-Pd system were investigated by Dublon and Yeshurun.[16] They too obtained a phase diagram similar to that of the SK model. A scaling analysis was again applied near the FM-SG transition. The value for $\tilde{\delta}$ is less than in Ref. 13, but the isotherms do satisfy the magnetic equation of state, within experimental error. Although no conclusion was made as to the nature of the transition, the success of the scaling analysis is consistent with it being a continuous phase transition.

Low field measurements on the Fe-Mn system were done by Manheimer et al.[13] Measurements were taken in the field range 1 to 10 Oersteds. Their conclusion was that $M \to 0$ at $T \to T_{fg}^{+}$ and $T \to T_{pf}^{-}$. Also, the susceptbility $\chi \to \infty$ at $T \to T_{fg}^{-}$ and $T \to T_{pf}^{+}$. This is evidence of a double transition behavior. They too concluded that the FM-SG transition is a true equilibrium phase transition. Investigations done on the Gd-La system by Sellmyer and O'Shea[17-18] also revealed double transition behavior. The multicritical point for this system occurs at about 67at.% Gd which is about the same as in the Fe-Mn system.

Chapter 3

EXPERIMENTAL ASPECTS

3.1 Sample Preparation

The systems under study in this work have the following stoichiometry; $Gd_xTM_{72-x}G_{28}$ where TM = Mn, Ni, La and $G_{28} = Ga_{18}B_{10}$ and is a non-magnetic glass former.

A. Alloy Preparation

Elements required to make an alloy are first weighed according to their atomic composition in the correct stoichiometry. The weighted elements are then combined to be melted into an alloy. An arc furnace as shown schematically in Fig. 2a is used for this purpose. The elements are placed on a copper anode with smaller chips covered by larger pieces to avoid the smaller ones flying away during melting.

The compound is melted in an argon-rich chamber after pumping and flushing it three times with argon to minimize oxidization during melting. An electrode with a pointed tip is supplied with current in the range of 10A to 30A from a power supply to melt the compound. An arc is struck by positioning the electrode tip near the copper anode. A homogeneous mixture is insured by moving the arc over the sample. Sample melting is usually less than 10 seconds to avoid loosing elements through evaporation. The mass loss in the Gd-Ni and Gd-La systems ranges between 0.01% to 0.2% and for the Gd-Mn system between 0.1% to 1%. Samples with more than 1% mass loss are not used. Better homogeneity is ensured by turning the sample over and remelting.

B. Preparing the Amorphous Solid

There are a number of techniques used in preparing amorphous

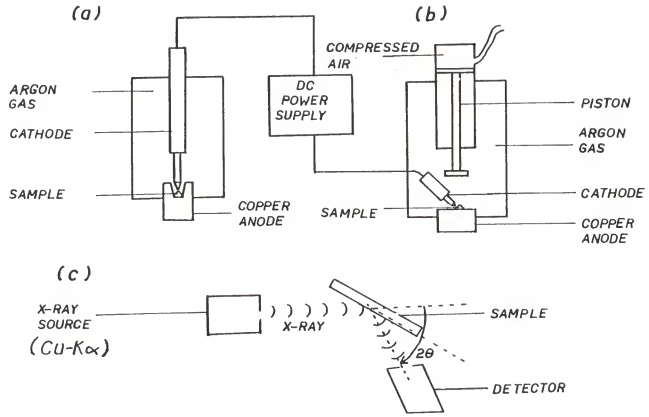

Figure 2: Schematics for sample preparation and characterization apparatus. (a) The arc furnace, (b) the splat cooling, and (c) the X-ray apparatus.

solids. Most commonly used techniques include sputtering, evaporation, melt-spinning and splat-cooling (the hammer and anvil) techniques.

The method used in this work is the splat cooling technique[17-18] which is shown schematically in Fig. 2b. A small piece of the alloy weighing about 200 mg prepared earlier is placed on the copper anvil. As was done in the arc furnace, the electrode's tip is placed near the copper anode to strike an arc. Current through the electrode is adjusted between 16A and 18A. When the sample is melted, a trigger is released, removing the electrode and pressing the molten alloy onto the copper anvil. It takes about 1ms for the trigger to drop to the sample and on contact, decreased the sample's temperature by 1000 degrees Kelvin. As a result, a cooling rate of $\sim 10^6$ K/s is attained. The sample obtained is in the form of a circular disc about 3.5cm in diameter and 50 microns thick. One advantage this technique has over melt spinning is that there are two cooling surfaces to quench the molten alloy leading to the achievement of high cooling rates with comparatively simple apparatus.

3.2 Sample Characterization

A. X-ray Analysis

Structure of the samples is examined by X-ray diffraction. Samples measuring about 1cm x 2cm are placed on glass slides and mounted onto the apparatus as shown in Fig. 2c. Cu-Kα radiation is used as the X-ray source. A proportional counter is used for detecting diffracted signals.

As a check, a permaquartz sample is run and sharp diffracted peaks are observed as illustrated in Fig. 3b, characteristics of the dif-

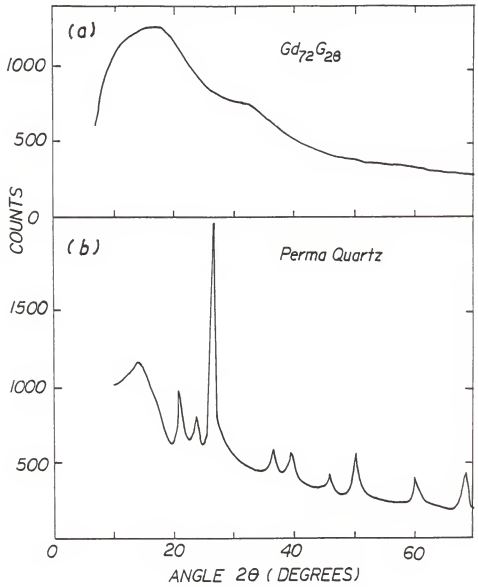

Figure 3: X-ray diffractograms for (a) the X = 72 sample, (b) the perma-quartz, (c) the X = 64 sample of the Gd-Ni system, and (d) the X = 64 sample of the Gd-Mn system illustrating the difference between crystalline and amorphous structure.

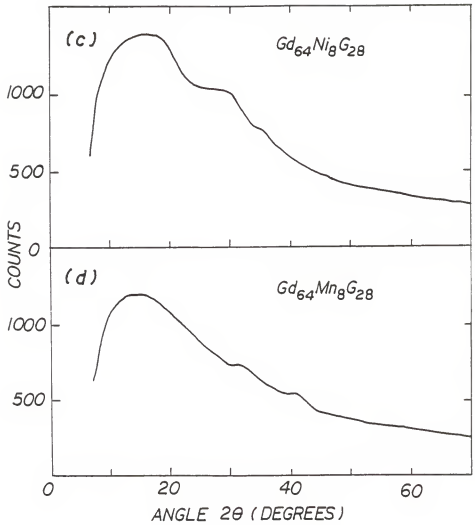
(c)
$Gd_{64}Ni_8G_{28}$
1000
500
0
COUNTS
(d)
$Gd_{64}Mn_8G_{28}$
1000
500
0
20
40
60
ANGLE 2θ (DEGREES)

fraction pattern of a crystal. In contrast, diffractograms of samples in this work showed broad and diffuse peaks. No sharp peaks are observed. The absence of any sharp peaks assured us that the sample is amorphous. Microscrystallinity may be present but electron microscopy should be done on the samples to determine this. Detailed structural studies of the samples is not the objective of this work. Diffractograms of some of the samples used in this work are shown in Fig. 3

B. Differential Scanning Calorimetry (DSC)

In addition to X-ray analysis, samples are examined for glass stability. Using the DSC, samples are heated to temperatures as high as 720°C. Glass stability is checked for by checking occurrence of crystallization indicated by an exothermic reaction.[28] Samples weighing between 5 mg and 6 mg are sandwiched between two copper pellets. A standard copper pellet with no sample in it is used as a reference. Both the pellets are set inside the calorimeter ensuring that they are not touching each other. The pellets are heated at a rate of 20K/min in an argon-rich chamber to minimize oxidation.

For the X = 72 sample, a small exothermic peak occurs at a temperature of about 710K indicating partial crystallization, followed by a large sharp exothermic peak at a higher temperature indicating full crystallization. These two peaks remain at about the same intensity with the peak temperatures shifted down on going from the X = 72 to the X = 66 sample in the Gd-La system as illustrated in Fig. 4a. A different behavior is observed for the Gd-Ni system where the sharp peak observed at high temperature for the X = 72 sample, slowly vanishes as X is decreased as illustrated in Fig. 4b. This peak is absent for X < 60. Instead, the smaller peak that was observed in the

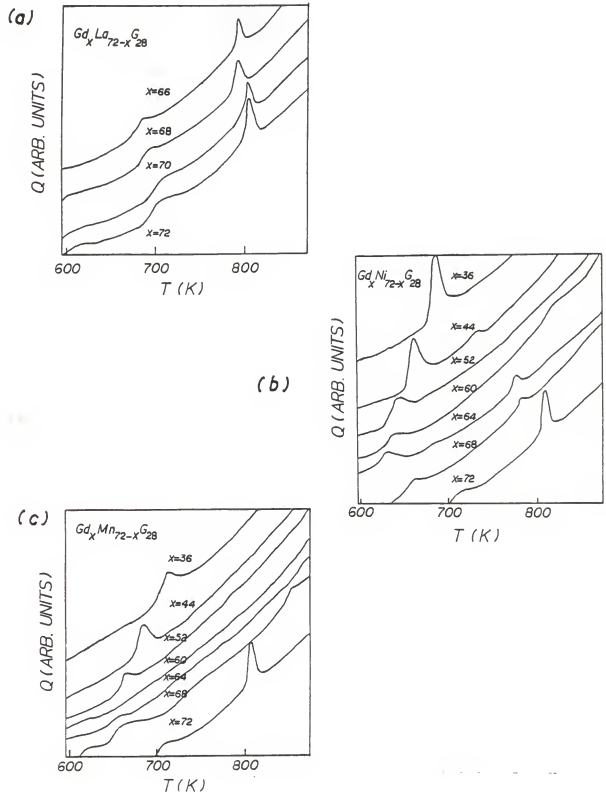

Figure 4: Differential scanning calorimetry measurement of heat flow Q as a function of temperature T for the (a) Gd-La, (b) Gd-Ni, and (c) Gd-Mn systems with the zeros shifted for each X in each system.

X = 72 sample appears to get larger with smaller X. The peak temperature for this peak increases as X is decreased. This behavior is similar to the Gd-Mn system except that for the Gd-Mn system the sharp peak vanishes for the X = 64 sample as shown in Fig. 4c in this system. The glass transition temperature as seen in the sharp peak increases for lower X suggesting that the glass is becoming more stable. The amplitude of the peak however, did not show a steady increase as was found in the Gd-Ni system.

The difference in behavior between Gd-La and Gd-Ni or Gd-Mn can be attributed at least in part to the size of the atoms. La is a rare-earth and so the ions are close in size to those of Gd. On the other hand, Mn and Ni are transition metals and are smaller in size, hence the similar behavior for Gd-Ni and Gd-Mn systems. The dependence of crystallization temperature on the size of the alloying element is not well understood at the moment.

3.3 Measurement Technique

A. Vibrating Sample Magnetometer (VSM)

The dc magnetization M is measured in this technique. As shown in Fig. 5a, a probe driven by a mechanical driver vibrates with a vertical amplitude A and frequency 37 Hz. Mounted on the probe is a set of reference modulation coils supplied with a dc signal of about 200 mA. The signal induced by this dc coil is picked up by a set of reference pick-up coil and is given by

$$V_R = k_R \omega A (\exp i\omega t) M_R$$

where ω is the frequency of vibration, k_R a geometric constant and M_R a constant reference magnetic moment. Similarly, the sample's pick-up coil sees a voltage

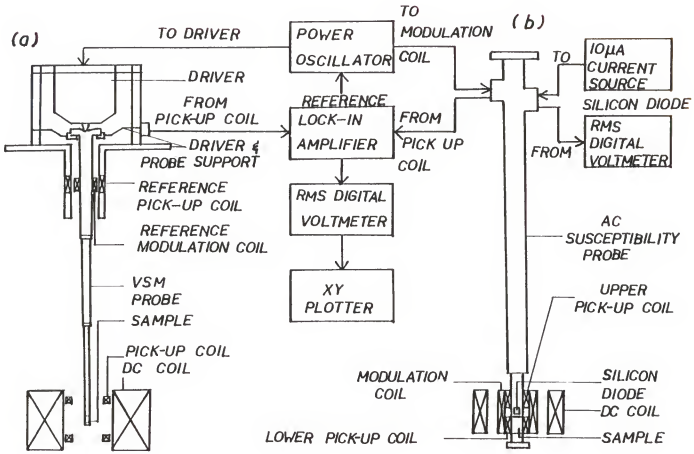

Figure 5: Schematics of the apparatus used for measuring the magnetic properties. (a) Vibrating sample magnetometer (the thermometry is not drawn), and (b) AC susceptibility.

$$V_S = k_S \omega A (\exp i\omega t) M_S .$$

The reference signal V_R is kept constant and checked periodically throughout all measurements. The sample signal is proportional to the magnetization of the sample as shown in the above equation.

The sample (and reference) pick-up coil are wound in series opposition so that the signal from the sample in each half of the sample pick-up coils add. During vibration, the sample enters one half of the coil while leaving the other half of the coil. In addition, any external noise will induce a net zero signal in the coil. The ac output signal is converted to a dc signal by the lock-in analyzer and monitored by a digital voltmeter and an X-Y plotter. A magnet coil capable of providing a dc magnetic field of 500 0e is used. Samples used are in the form of long strips measuring about 1mm x 0.05mm x 10mm. Strips weighing about 30mg are inserted inside a sample holder about 2mm in diameter and 10mm long. When taking measurements, the long axis of the sample is placed parallel to the applied magnetic field to reduce demagnetization effects as shown in Fig. 5c.

In this work a Janis cryostat is used for low temperature measurements. The VSM probe is suspended in a sample chamber which is pumped and flushed before cooling down with helium gas to avoid ice formation. Two different diodes are used to monitor the temperature. A Si diode is placed near the sample at the end of the VSM probe for monitoring the sample's temperature. The temperature in the chamber is lowered by allowing cold helium gas from the liquid helium chamber to enter the sample chamber via a needle valve. A heater with a Ga-As diode placed near it is used for changing the temperature. Current through the heater is set by setting the voltage on the heater con troller for the Ga-As diode corresponding to the desired temperature.

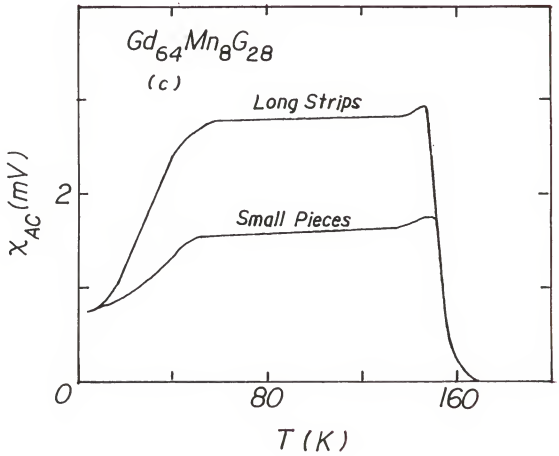

Figure 5: (c) Long strips compared to small pieces for the X = 64 sample of the Gd-Mn system to illustrate the demagnetization effects.

B. AC Susceptibility

Internal susceptibility χ is measured by measuring $\chi_{ac} = \partial M/\partial H_a$ where H_a is an applied field. The internal field H is related to the applied field by

$H = H_a - NM$ where N is a demagnetization factor. Internal susceptibility is then given by

$$\chi^{-1} = \chi_{ac}^{-1} - N$$

which can be rewritten as

$$\chi = \chi_{ac} / (1 - N\chi_{ac})$$

Two limits may be considered:

$$\lim \chi \to \infty;\ \chi_{ac} \to 1/N$$

and $\lim \chi \to$ small; $\chi_{ac} \to \chi$

Measurements are made by setting up the apparatus as shown schematically in Fig. 5b. Two sets of coils are wound onto a Delrin coil former. A set of modulation coils provide an AC field. The pick-up coil is wound in series opposition to cancel any direct pick-up from the modulation coil. The pick-up coil is balanced to within two turns (each coil has 585 turns). Without any sample in the lower half of the pick-up coil, the signal induced in the upper and lower halfs of the coil cancels out.

A lock-in analyzer is used to supply an oscillating current to the modulation coil. The signal induced in the pick-up coil is fed back to the lock-in-analyzer, converted to a dc signal and amplified. The phase on the analyzer is set to maximize the output signal which is then monitored by a digital voltmeter and an X-Y plotter.

The sample's temperature is monitored by a silicon diode placed close to the sample. Temperature conversion from the diode's voltage is provided by the manufacturer. A 10 μA current source is used for

this diode and its voltage is recorded by a digital voltmeter and an X-Y plotter.

Measurements are taken at a frequency of 280Hz and an RMS ac field of about 1 Oe. The temperature is changed by raising and lowering the ac susceptibility probe mechanically. A dc motor is used for this purpose. Samples used are those prepared for the VSM and the samples are placed in the lower half of the pick-up coil when taking measurements.

Chapter 4

MAGNETIC BEHAVIOR AND THE MAGNETIC PHASE DIAGRAMS OF Gd-rich SYSTEMS

4.1 Introduction

Using the ac susceptibility apparatus as described in the previous chapter, susceptibility $\chi_{ac} = \partial M/\partial H_a$ of the samples is measured. Samples used in the measurements are in the form of long strips with their long axes parallel to the applied dc field to minimize demagnetization affects. The higher Mn content (>20 at.%) samples tended to be brittle after quenching and broke up into smaller pieces. Hence, long strips were not available and resulted in higher demagnetization affects as illustrated in Fig. 5c for these samples.

4.2 AC and DC Susceptibility

The samples are cooled (in a 1 Oe ac field) by lowering the ac susceptibility probe into a liquid helium dewar. For the X = 72 sample, a sharp rise of χ_{ac} is observed at the PM-FM transition. It approaches the demagnetization limit and remains at this value until the SG state is entered at a lower temperature. Microscopically, spins which are randomly oriented, start to feel the molecular field from neighboring spins and start to align themselves. In the FM state $\chi \to \infty$ and since $\chi_{ac} = \chi / (1 + N\chi)$, $\chi_{ac} \to 1/N$. As the sample is further cooled, a sharp drop in χ_{ac} is observed at a fairly low temperature. This drop marks the entry into the SG state.

A. Gd-La System

AC susceptibility for the Gd-La system plotted in units of 1/N is shown in Fig. 6a. This system exhibits double transition behavior for $X \geq 68$ and a PM-SG transitions for $X < 68$. The transition tempera-

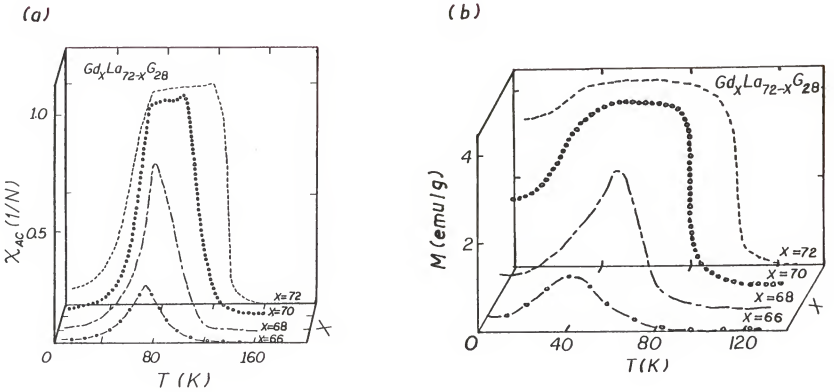

Figure 6: (a) A quasi-three-dimensional plot of the ac susceptibility done in an RMS field of 1 Oe and plotted in units of 1/N, and (b) the dc magnetization done in a dc field of 1.8 Oe for the Gd-La system.

tures T_{pf} and T_{fg} are observed to decrease and increase respectively for a decrease in X. For the X = 66 sample, only a PM-SG transition is observed. The disappearance of double transition behavior is believed to be related to an increase in exchange fluctuations as the La content is increased resulting in increased frustration effects in the system.

Magnetization of this system for samples cooled in a dc field of 1.8 Oe shown in Fig. 6b exhibit similar behavior to that of ac susceptibility. Here, the microscopic magnetization M rises continuously below T_{pf} to a maximum value and remains high over a wide range of temperatures before dropping down at T_{fg} indicating clearly the effects of frustration in this system. For the X = 68 sample, only a single peak is observed. Although this is characteristic of a PM-SG transition, scaling analysis done on the sample reveal a double transition behavior. For the X = 66 sample, the maximum amplitude of X_{ac} and M is much smaller than the other samples. Frustration effects are very strong for this sample and indicate the presence of significant antiferromagnetic interactions.

B. Gd-Ni System

AC susceptibility and dc magnetization for the Gd-Ni system is shown in Fig. 7. The transition temperatures T_{pf} and T_{fg} initially decrease as X is decreased. For the X = 64 sample, T_{fg} is observed to increase while T_{pf} still decreases. For the X < 56 samples, the double transition behavior present at higher X, starts to disappear. Only single peaks are observed for the X = 52,48 and 44 samples but the amplitude of the peaks remains close to the demagnetization limit. Double transition behavior is observed again for the X = 40,36 and 32 samples with the temperatures T_{pf} and T_{fg} shifted even lower. Values

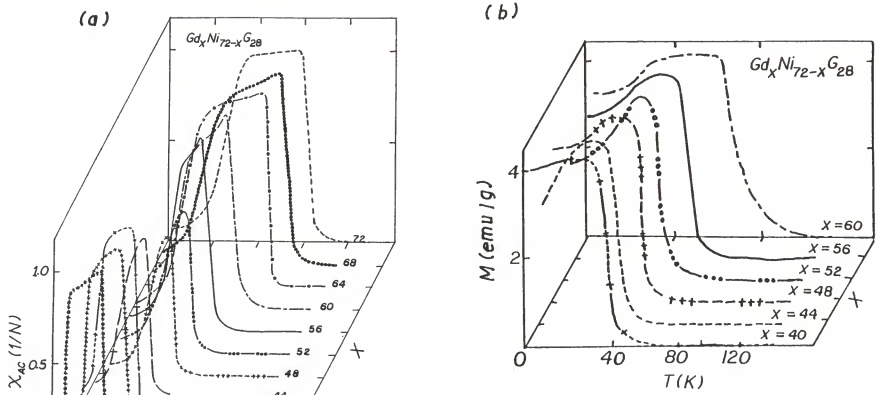

Figure 7: (a) A quasi-three-dimensional plot of the ac susceptibility done in an RMS field of 1 Oe and plotted in units of 1/N, and (b) the dc magnetization for various concentrations done in a dc field of 1.8 Oe for the Gd-Ni system.

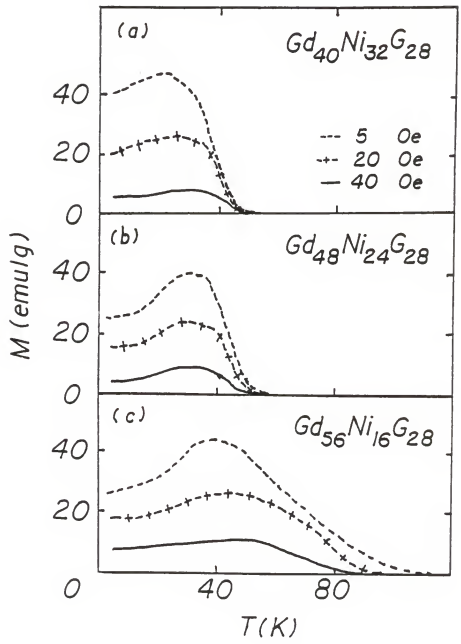

Figure 8: DC magnetization for the (a) X = 56, (b) X = 48, and (c) X = 40 samples of the Gd-Ni system cooled in fields of 5, 20, and 40 Oe.

of T_{pf} for these three samples are lower than the value of T_{pg} for the X = 44 sample. DC magnetization of the X = 40 sample cooled in a field of 1.8 Oe does not reveal a SG transition. This probably indicates weak SG behavior.

Increasing Ni content decreases the FM and SG ordering temperatures. For the X < 64 samples, the SG ordering temperatures increase while the FM ordering temperatures decrease. One might say that frustration effects have become stronger. Even though only a PM-SG transition is observed for the X < 56 samples, the frustration effects are not as strong as that in the Gd-La system judging from the amplitude of the peaks and the smaller decrease in ordering temperatures. It is not surprising that double transition behavior still persists for the X = 48 and 44 samples. Scaling analysis for the X = 52 sample reveals that double transition still exist. The presence of double transitions for the X = 40,36 and 32 samples supports the suggestion that double transition behavior does not disappear for the range of composition studied in this particular system. It has been found that Gd-Ni interactions are antiferromagnetic[32-33] and that Ni ions do not possess any moment below about 30 at.% Ni. It is possible though, that above this value, the Ni ions start to develop a moment when it is surrounded by other Ni ions, thus contributing to the strength of the FM ordering for the X < 40 samples. Figure 8 shows the magnetization behavior as a function of temperature for the X = 56,48 and 40 samples of the Gd-Ni system cooled in fields of 5,20 and 40 Oe. One obvious feature is that for the X = 40 sample, the FM-SG transition is not well-defined at 40 Oe indicating that the SG state is weaker.

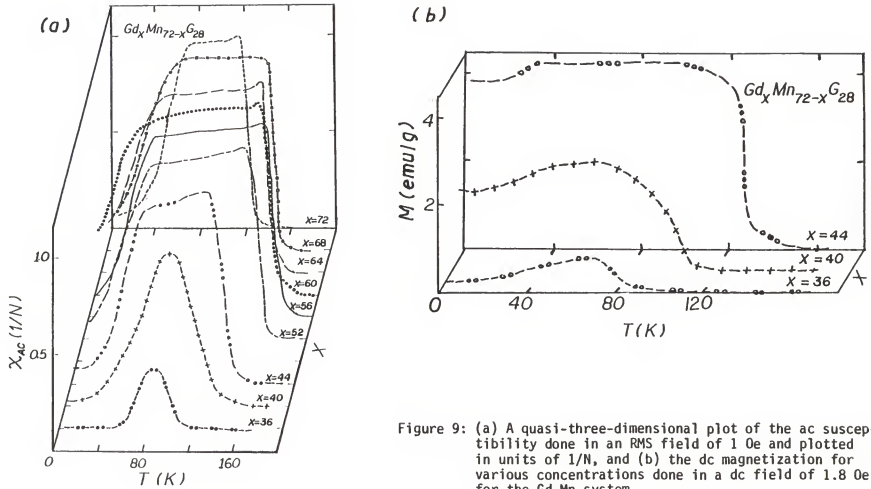

Figure 9: (a) A quasi-three-dimensional plot of the ac susceptibility done in an RMS field of 1 Oe and plotted in units of 1/N, and (b) the dc magnetization for various concentrations done in a dc field of 1.8 Oe for the Gd-Mn system.

C. Gd-Mn System

AC susceptibility and dc magnetization for the Gd-Mn system is shown in Fig. 9. Increasing the Mn concentration increases the PM-FM ordering temperatures for the $X \geq 56$ samples and decreases it for the $X < 56$ samples. For the X = 40 sample, a single peak is observed in both the ac susceptibility and dc magnetization although double transition behavior may still persist. This marks the onset of a PM-SG transition. The demagnetization factor for the X = 44,40 and 36 samples are large because these samples are in small pieces. When plotting the ac susceptibility for these three samples, the amplitude of the peaks were adjusted to the proper value to account for the large N. The X = 36 sample shows only a PM-SG transition with a small amplitude similar to the X = 66 sample in the Gd-La system.

For $X \geq 56$ the increase in FM ordering temperature may be attributed to the interaction between Gd and Mn moments. Interaction between Gd-Gd moments is ferromagnetic while interaction between Mn-Mn moments is antiferromagnetic. A small increase of Mn increases the ordering temperatures. It is known that in a number of other systems, the Gd-Mn interaction is antiferromagnetic. Then, an isolated Mn ion may polarize the Gd spins around it resulting in small ferromagnetic clusters. There is no significant Mn-Mn interaction at small concentrations and so the result is an increase in the ordering temperature. At higher Mn concentrations, it becomes more likely that a Mn will have a Mn nearest neighbor resulting in a frustration and consequent lowering of the ordering temperature. This is indicated by the decrease in T_{pf} and an increase in T_{fg} for the X = 52 sample. Further reduction in X, increases fluctuations in the exchange interactions.

The PM-SG transition sets in at about 38 at.% Gd. The transition temperature T_{pg} is generally higher than that of Gd-Ni system. In this (Gd-Mn) system, antiferromagnetic interactions are probably the source of the strong SG behavior.

4.3 The Magnetic Phase Diagrams

Phase diagrams for the three systems studied are shown in Fig. 10. The transition temperatures T_{pf} are chosen from the peak of χ_{ac} and from scaling analyses. A scaling analysis at T_{fg} (Sec. 5.2) gives the FM-SG transition temperature and for the X = 68 sample of the Gd-La system, this temperature corresponds to the point where χ_{ac} has dropped to approximately a quarter of its original height. This point is chosen as the FM-SG transition temperatures in the other samples of this work. The multicritical point of the Gd-La system is at about 68 at.% Gd. The dashed lines in Fig. 10 represent uncertain transition lines. As illustrated, double transition behavior exists above X = 67 at.%. For the Gd-Ni system, double transition behavior persists for all of the compositions studied. Although this is not obvious from susceptibility measurements, scaling analysis for the X = 52 and 56 samples (Sec. 5.2) reveal the existence of a double transition behavior. For the Gd-Mn system, the multicritical point is at about 38 at.% Gd. For X > 55, the FM ordering is strengthened for increasing Mn concentration. For X < 55, the phase diagram assumes similar behavior to that observed in other systems.[13-18]

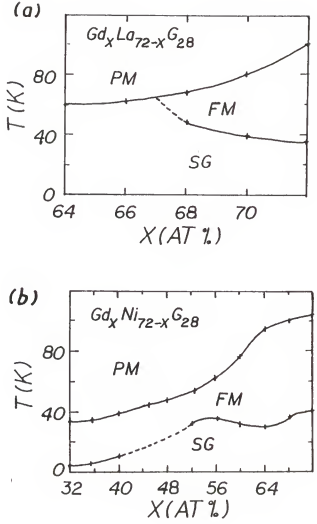

Figure 10: Magnetic phase diagrams for the (a) Gd-La, (b) Gd-Ni, and (c) Gd-Mn systems.

Chapter 5

CRITICAL BEHAVIOR AND THE SCALING ANALYSIS

5.1 Scaling Behavior Near the PM-FM Transition

Magnetization as a function of applied dc field is taken using the vibrating sample magnetometer. Based on the transition temperature obtained from ac susceptibility, the sample temperature is set about ten degrees above the transition temperature. The set temperature on the temperature controller is allowed to stabilize to within a tenth of a degree before an isotherm is taken. Starting with zero field, the magnetization is recorded as the magnetic field is slowly increased to the maximum value. The field is then turned off, the temperature is decreased and allowed to stablize before another isotherm is taken. Isotherms are taken at about two degrees apart. An example of magnetic isotherms close to the PM-FM transition for the X = 64 sample of the Gd-Mn system is shown in Fig. 11a. The limiting slope of the magnetization just below T_{pf} is equal to 1/N. An Arrott plot for this sample is shown in Fig. 11b. This is a plot of M^2 vs. H_a/M. As $T \rightarrow T_{pf}^+$, $H_a/M \rightarrow 1/\chi_{ac}$ and $H/M \rightarrow 1/\chi$. As the FM state is entered, $\chi \rightarrow \infty$ and $\chi_{ac} \rightarrow 1/N$, thus $H_a/M \rightarrow N$ which is the intercept on the H_a/M axis. The demagnetization factor for the sample discussed above is about 0.3 Oe g/emu. After correcting for demagnetization, the first isotherm that passes through the origin corresponds to the transition temperature T_{pf}. For $T < T_{pf}$, isotherms continue to intersect the origin and for $T > T_{pf}$, isotherms intercept the H/M axis.

The reduced magnetization $m = M(\varepsilon,H) / |\varepsilon|^{\beta}$ and reduced magnetic field $h = H(\varepsilon,M) / |\varepsilon|^{\beta\delta}$ for the X = 64 sample of the Gd-Mn system is

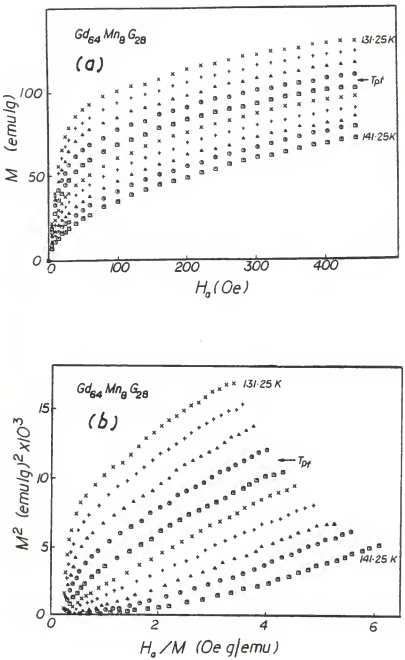

Figure 11: (a) Magnetic isotherms, and (b) an Arrott plot for the X = 64 sample of the Gd-Mn system near the PM-FM transition. The magnetic field has not been corrected for demagnetization effects.

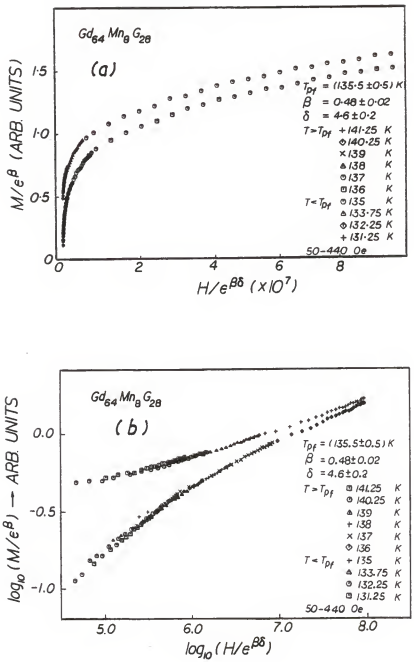

Figure 12: (a) Magnetization vs. magnetic field in reduced units for the X = 64 sample of the Gd-Mn system, and (b) a logarithmic plot of the reduced magnetization vs. reduced magnetic field to resolve the lowest field scaling behaviour near the PM-FM transition.

shown in Fig. 12a. In addition, a logarithmic plot is shown in Fig. 12b to resolve scaling behavior at lowest fields. The scaling analysis is done for fields above 30 Oe. Below 30 Oe, demagnetization affects are large. Thus the magnetization below this field will not scale properly. For this sample, there are six isotherms above T_{pf} and four isotherms below T_{pf}. As illustrated in Fig. 12, all six isotherms above T_{pf} collapse onto the lower branch while the four isotherms below T_{pf} collaspe onto the upper branch. The quality of scaling obtained is good suggesting a continuous phase transition.

Figures 13 to 16 show scaling analyses for the three systems studied in this work. They are plotted logarithmically to resolve scaling behavior at low fields. The values of T_{pf} for the samples obtained from Arrott plots are varied within experimental error to obtain good scaling. The values of β and δ are varied in the range of 0.2-0.6 and 2-6 respectively. The demagnetization correction to obtain the internal field is made before scaling the data. The values of β and δ of this work and those from previous work are summarized in Table 2.

The value of β in all of the analyses is fairly close to the mean field value. This value is larger than those found in all transition metal metallic glasses but are close to that of the Gd-La[18] system. On the other hand, values of δ agree fairly closely with the values found in other metallic glasses.[13-18] The value of β for the X = 72 sample is close to that of Ref. 18 but the value of δ in this work is closer to that of crystalline Fe. The value of δ in all of the analyses for the systems in this work ranges from 4.4 to 5.0 which are close to the values for crystalline Ni and the d = 3 heisenberg model respectively. The scaling behavior near this transition are good

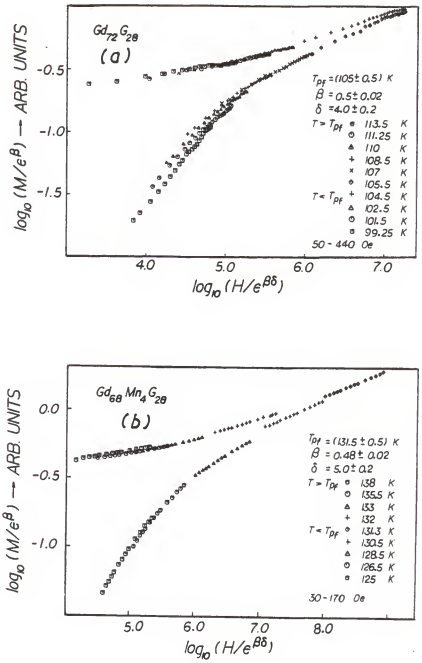

Figure 13: Logarithmic plots of magnetization vs. magnetic field in reduced units for (a) the X = 72 sample, and (b) the X = 68 sample of the Gd-Mn system near the PM-FM transition.

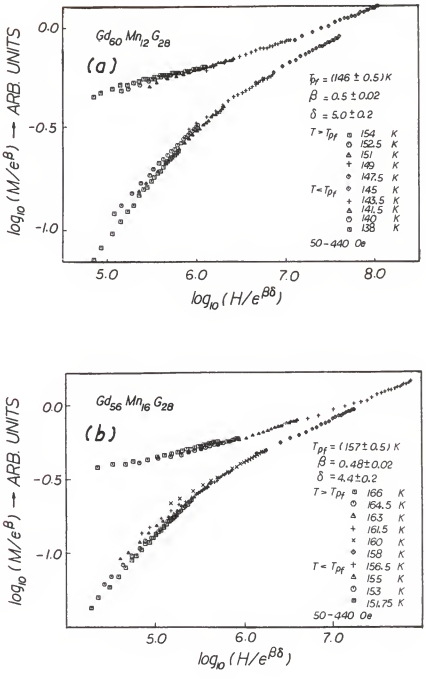

Figure 14: Logarithmic plots of magnetization vs. magnetic field in reduced units for (a) the X = 60 sample, and (b) the X = 56 sample of the Gd-Mn system near the PM-FM transition.

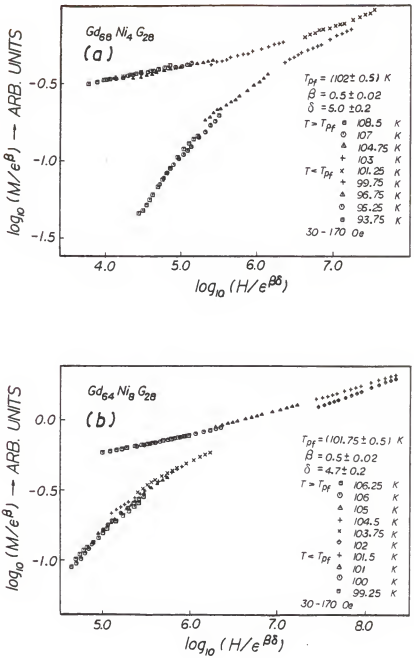

Figure 15: Logarithmic plots of magnetization vs. magnetic field in reduced units for (a) the X = 68 sample, and (b) the X = 64 sample of the Gd-Ni system near the PM-FM transition.

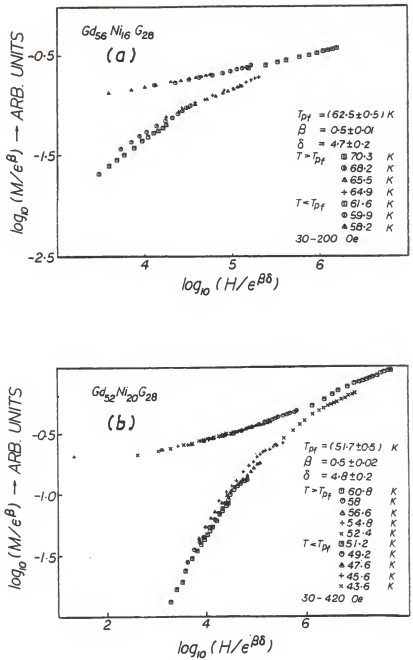

Figure 16: Logarithmic plots of magnetization vs. magnetic field in reduced units for (a) the X = 56 sample, and (b) the X = 52 sample of the Gd-Ni system, and (c) the X = 68 sample of the Gd-La system near the PM-FM transition.

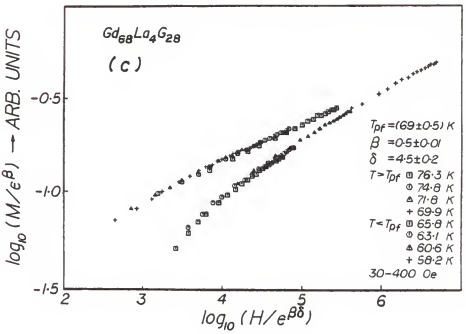
$Gd_{68}La_4G_{28}$
(c)
T_{pf}=(69±0·5) K
β =0·5±0·01
δ =4·5±0·2
T>T_{pf} 76·3 K
74·8 K
71·8 K
69·9 K
T<T_{pf} 65·8 K
63·1 K
60·6 K
56·2 K
30-400 Oe
$log_{10}(M/\varepsilon^{\beta})$ → ARB. UNITS
$log_{10}(H/\varepsilon^{\beta\delta})$
-0·5
-1·0
-1·5
2
3
4
5
6

Table 2: Summary of the experimental values of critical exponents for metallic glasses near the PM-FM transition. The numbers in bracket are the uncertainties in the least significant digit.

System	α	β	γ	δ	T_c	Ref.
$Co_{70}P_{20}B_{10}$	-0.14(5) -0.18(4)	0.40(1)	1.34(2.5)	4.39(5)	452.30(7)	34 35
$Fe_{32}Ni_{36}Cr_{14}P_{12}B_6$	-0.49(12) -0.19(9)	0.41(2) 0.43(2) 0.42(4)	1.67(5) 1.33(5) 1.35(3)	5.07(20) 4.43(17) 4.3(2)	254.5(10) 250.0(10) 249.0(1)	36 See Ref. 1 of Ref. 40 37
$Fe_{80}P_{13}C_7$	-0.06(9)	0.38(2)	1.30(5)	4.47(5)		38
$Fe_{29}Ni_{49}P_{14}B_6Si_2$	-0.05(8)	0.40(1)	1.70(1)	5.25(1)	384.5	39
$Fe_{40}Ni_{40}P_{14}B_6$	-0.07(4)	0.38(1)	1.31(2)	4.46(4)	519.9(2)	See Ref. 3 of Ref. 40
$Fe_{20}Ni_{60}P_{14}B_6$		0.39(2)	1.33(5)	4.45(7)	227.7(5)	See Ref. 2 of Ref. 40
$Fe_{13}Ni_{67}B_{19}Si_1$		0.42(2)	1.35(4)	4.48(5)	268.5(2)	40
$(Fe_{1-x}Mn_x)_{75}P_{16}B_6Al_3$						
x = 0.2, 0.3, 0.32		0.40(3)		~5.1(3)	See Ref.	41
x = 0.36		0.40(5)		2.5(5)	42(2)	
$(Fe_{1-x}Ni_x)_{75}P_{16}B_6Al_3$						
x = 0.2		0.35(3)		4.3(4)	600(4)	
x = 0.6, 0.65, 0.75, 0.80		0.40(5)		5.0(4)	See Ref.	

Table 2 (continued)

$(Co_{1-x}Mn_x)_{75}P_{16}B_6Al_3$					
x = 0.2	~0.40(4)		5.2(4)	298(3)	
x = 0.3	0.40(4)		5.0(4)	110(2)	
$(Co_{1-x}Ni_x)_{75}P_{16}B_6Al_3$					
x = 0.4, 0.5, 0.6, 0.62, 0.64, 0.66	~0.40(4)		5.0(4)	See Ref.	
x = 0.68	0.40(4)		4.0(4)	28(2)	
$(Fe_{1-x}Mo_x)_{75}P_{16}B_6Al_3$					
x = 0.15, 0.20	0.41(2)		4.8(1)		42
$Fe_xPd_{82-x}Si_{18}$					
$x \leq 20$	0.40(3)		5.0(4)		16
$(Fe_xMn_{1-x})_{75}P_{16}B_6Al_3$					
x = 0.65, 0.7, 0.8	~0.40	~1.5	4.75		13
$Fe_{80-x}Cr_xB_{20}$					
x = 15		1.43(5)	~4.1(3)	225.6(2)	43
x = 20		1.55(5)	4.20(3)	120.20(15)	
x = 25		1.58(5)	5.25(25)	33.20(5)	
x = 27, 28			6.35-7.0		

Table 2 (continued)

$Gd_{80}Au_{20}$	-0.17(4)	0.44(2)	1.29(5)	3.96(3)	149.45(20)	30
Gd_2Co	~0	0.41(2)	1.16(5)	3.60(10)	172(3)	31
$Gd_{72}Ga_{18}B_{10}$	-0.74(6)$^+$	0.48(2)	1.60(4)	4.7(2)	112(1)	18
$Gd_{68}La_4Ga_{18}B_{10}$	-0.53(6)$^+$	0.46(2)		4.5(2)	76.0(5)	18
$Gd_{72}Ga_{18}B_{10}$	-0.50(6)$^+$	0.50(2)		4.0(2)	105.0(5)	This work.
$Gd_{68}La_4Ga_{18}B_{10}$	-0.75(6)$^+$	0.50(1)		4.5(2)	69.0(5)	
$Gd_xMn_{72-x}Ga_{18}B_{10}$						
x = 68	-0.88(6)$^+$	0.48(2)		5.0(2)	131.5(5)	
x = 64	-0.69(6)$^+$	0.48(2)		4.6(2)	135.5(5)	
x = 60	-1.00(6)$^+$	0.50(1)		5.0(2)	146.0(5)	
x = 56	-0.59(6)$^+$	0.48(2)		4.4(2)	157.0(5)	
$Gd_xNi_{72-x}Ga_{18}B_{10}$						
x = 68	-1.00(6)$^+$	0.50(2)		5.0(2)	102.0(5)	
x = 64	-0.85(6)$^+$	0.50(2)		4.7(2)	101.7(5)	
x = 56	-0.85(6)$^+$	0.50(2)		4.7(2)	62.5(5)	
x = 52	-0.90(6)$^+$	0.50(2)		4.8(2)	51.7(5)	

$^+$Calculated from the measured critical exponents [$\alpha = 2 - \beta(\delta+1)$]. The uncertainties for α are calculated from uncertainties of β and δ and combining them in quadrature.

suggesting a continuous phase transition. It has been shown that a sharp transition is one with negative values of the critical indices α while positive α suggest smeared transition. The values of α in this work, calculated from values of β and δ obtained experimentally are negative. This is consistent with a sharp phase transition as found in other metallic glasses.[13-18]

5.2 Scaling Behavior Near the FM-SG Transition

Close to the FM-SG transition, hysteresis appears and the magnetization at a particular temperature and magnetic field depends on the previous history of the sample. This complicates a scaling analysis considerably since the equilibrium magnetization must be used. Both computer simulations and experimental observations indicate that the field cooled magnetization to be the equilibrium magnetization (simulations and experiments show no time dependence for the field cooled magnetization and a strong time dependence for the initial magnetization at low temperatures, $T \leq (T_{fg}/2)$.

To measure the initial magnetization, the same procedure used near the PM-FM transition is followed. Isotherms are taken at two degrees intervals. However, below 30K, remanent magnetization becomes large. Thus below this temperature the sample is warmed up to about 60K, cooled down to the desired temperature and the isotherms are taken when the temperature stabilizes. This procedure must be followed for every isotherm where remanent magnetization is relatively large. The field cooled magnetization is measured by cooling the sample at about 2K/min in a given magnetic field. The difference between the initial and field cooled magnetization is illustrated in Fig. 17a. It is clear that hysteresis effects are present near this transition and these are characteristic of a SG phase transition. We also see a

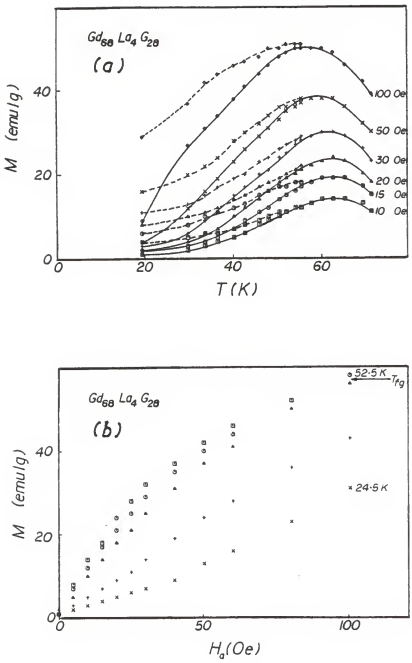

Figure 17: (a) Comparison of the field cooled (dashed lines) and initial magnetization (solid lines) data, and (b) selected magnetic isotherms for the X = 68 sample of the Gd-La system near the FM-SG transition.

time-dependence of the magnetization at low temperatures as expected for a SG system.

In the absence of any theory to compare to, the static scaling hypothesis is applied near the FM-SG transition. The demagnetization factor obtained at the PM-FM transition is used near the FM-SG transition to correct for demagnetization effects. The transition temperature T_{fg} along with $\tilde{\beta}$ and $\tilde{\delta}$ are varied accordingly to obtain the best scaling. The scaling analysis at this transition (FM-SG) is somewhat more difficult than at the PM-FM transition for a number of reasons. As discussed below, very low field measurements (<200 Oe) are required, hysteresis is present at this transition and liquid Helium is required since the transition is below nitrogen temperatures. Therefore, a few samples are carefully selected to do a scaling analysis on. The X = 68 sample of the Gd-La system is studied to compare it to previous work and the X = 56 and 52 samples of the Gd-Ni system are chosen since this system shows an unusual phase diagram. The initial magnetization isotherms for the X = 68 sample of the Gd-La system are shown in Fig. 17b. One obvious feature near this lower transition is that the magnetization is observed to decrease with temperature instead of the regular increase with temperature as observed near the upper transition.

The scaling analysis for the X = 68 sample of the Gd-La system is shown in Fig. 18. The collapse of the isotherms onto two branches is well-defined. Note that the lower branch corresponds to $T < T_{fg}$. It is found that both the initial and field cooled magnetization yield the same values of $\tilde{\beta}$ and $\tilde{\delta}$ as indicated in Table 3 (approximately 0.47 and 3.1 respectively), within experimental error. At about 200 Oe, systematic departures from scaling start to become apparent. This is

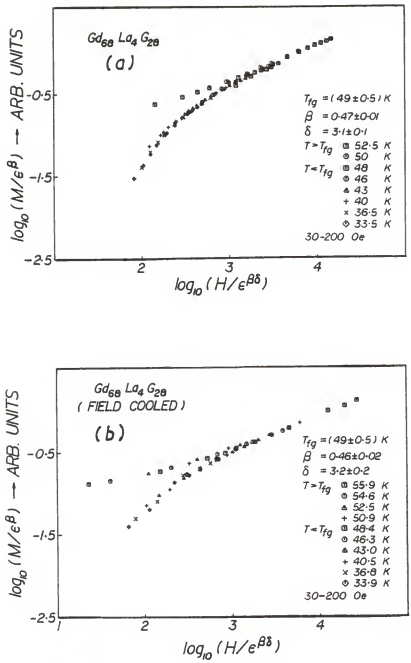

Figure 18: Logarithmic plots of magnetization vs. magnetic field in reduced units for (a) the initial magnetization data, and (b) the field cooled data for the X = 68 sample of the Gd-La system near the FM-SG transition.

not a cause for concern since good scaling is expected only in the limit of small magnetic fields (and also small reduced temperatures). It is interesting to note that no deviations from scaling at the upper transition are found up to 440 Oe and other workers have shown that good scaling may be obtained up to 20,000 Oe.[18] Below about 30 Oe the demagnetization correction becomes so large that it cannot be applied with any amount of certainty and the noise in the data (actually in H) becomes too large to resolve any scaling.

In the case of the Gd-Ni system, the initial magnetization for both the X = 56 and X = 52 samples show a well-defined scaling as shown in Fig. 19. The field below which scaling occurs here is less than 100 Oe and this shows that only small fields is needed to destroy the SG behavior. The critical exponents for these systems along with values measured in other systems are summarized in Table 3. The values of $\tilde{\beta}$ range from 0.47 to 0.50 in the Gd-La and the Gd-Ni systems and are the same, within experimental error, to those at the upper transition. The values of $\tilde{\delta}$ range from 4.1 to 4.3 and are somewhat lower than the values of δ at the upper transition.

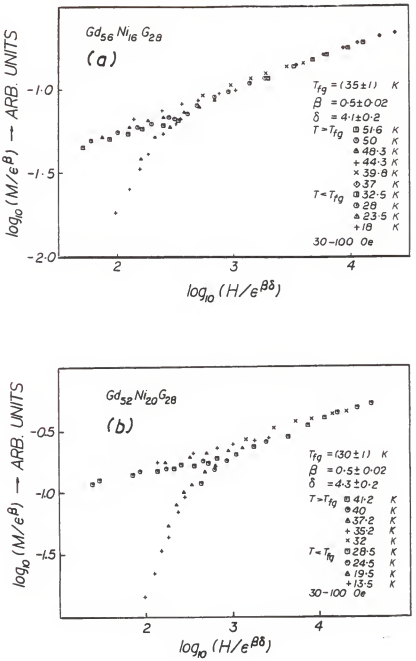

Figure 19: Logarithmic plots of magnetization vs. magnetic field in reduced units for (a) the X = 56 sample, and (b) the X = 52 sample of the Gd-Ni system near the FM-SG transition.

Table 3: Experimental critical exponent values at the FM-SG transition in transition metal and Gd-rich metallic glasses. The symbol G_{28} represents the combination $Ga_{18}B_{10}$ and G'_{25} the combination of $P_{16}B_6Al_3$. All data is for initial magnetization unless otherwise indicated. The numbers in bracket are the uncertainties to the least significant digit.

System	$\tilde{\beta}$	$\tilde{\delta}$	$\tilde{\delta}$	T_{fg}(K)	Ref.
$(Fe_{1-x}Mn_x)_{75}G'_{25}$					14
x = 0.30	0.40(3)		4.5(3)	31(2)	
x = 0.32	0.40(3)		4.5(3)	38(2)	
$(Fe_{0.2}Ni_{0.8})_{75}G'_{25}$	0.48(6)		4.8(6)	21(2)	
$(Co_{0.7}Mn_{0.3})_{75}G'_{25}$	0.38(5)		4.8(6)	38(3)	
$(Fe_xMn_{1-x})_{75}G'_{25}$					13
x = 0.65, 0.70	~0.40	~1.5	~4.75	65, 49	
$Fe_xPd_{82-x}Si_{18}$					16
x = 9, 10, 12	0.40(3)		3.5(3)	18(1)*	
$Gd_{72}G_{28}$	0.40(2)		4.0(3)	40(3)	18
$Gd_{68}La_4G_{28}$	0.40(2)		3.1(3)	44(3)	
$Gd_{56}Ni_{16}G_{28}$	0.50(2)		4.1(2)	35(1)	This work.
$Gd_{52}Ni_{20}G_{28}$	0.50(2)		4.3(2)	30(1)	
$Gd_{68}La_4G_{28}$	0.47(2)		3.1(1)	49.0(5)	
$Gd_{68}La_4G^{+}_{28}$	0.46(1)		3.2(2)	49.0(5)	

$^{+}$Field cooled magnetization data.

*For the x = 10 sample.

Chapter 6

DISCUSSION AND CONCLUSION

In all of the three systems studied in this work, double transition behavior is observed. Although computer simulations do not produce this behavior, experimental observations in other metallic glasses and Gd-rich glasses reveal that this behavior exists. AC and dc susceptibility measurements of the systems in this work show continuous changes in χ_{ac} and M near the transition temperatures T_{pf} and T_{fg}. It is also observed that hysteresis effects and long time dependent magnetization exist in the SG state indicating the non-equilibrium behavior of this state. The multicritical point for the Gd-La system and the Gd-Mn systems are at about 67 at.% and 38 at.% Gd respectively for the Gd-La system, the multicritical point is the same as that found by O'Shea and Sellmyer.[18] In the Gd-Ni system, even though susceptibility measurements of the X = 52,48 and 44 samples show single peaks, scaling analysis for the X = 52 sample reveal that double transition behavior still exists.

The static scaling hypothesis is applied to both the PM-FM and FM-SG transitions. Near both transition lines, it is observed that the isotherms collapse according to the static scaling hypothesis. The values of β for all of the samples that were studied are about 0.5 and this value is the same as $\tilde{\beta}$ for the samples X = 68 of the Gd-La system and X = 56 and 52 of the Gd-Ni system. On the other hand, the values of δ are apparently not constant and range from 4.0 to 5.0. At the FM-SG transition, $\tilde{\delta} \sim 4.2$ but this value is different from δ found

at the PM-FM transition for the same samples of the Gd-Ni system. The value of $\tilde{\delta}$ for the X = 68 sample of the Gd-La system is smaller ($\tilde{\delta}$~3.1) than that found for the Gd-Ni system. It is also interesting to note that the SG behavior is destroyed by magnetic fields of about 200 Oe in this system. This field is smaller (~100 Oe) for the Gd-Ni system.

The constant value of $\beta(\tilde{\beta})$ is in agreement with the universality hypothesis[8] which states that the critical exponents do not depend on the details of the microscopic interactions in the system but on the symmetry of the Hamiltonian and the dimensionality of the system. Such behavior has been observed in crystalline systems at the PM-FM transition where values of β of about 0.38 are found (see Table 1b). The wide variation in values of $\delta(\tilde{\delta})$ in this work is not understood but similar variations have been found in crystalline system at the PM-FM transition.

We conclude that double transition behavior exists in the Gd-rich metallic glasses studied in this work and the PM-FM and FM-SG transitions show the scaling behavior required by the static scaling hypothesis.

References

1. A.I. Gubanov, Fiz. Tver. Tela 2, 502 (1960).
2. Praveen Chaudhari, Bill C. Giessen and David Turnbull, Scientific American, April (1980).
3. P. Duwez, R.H. Wellens, W. Clement, J. Appl. Phys. 31, 1136 (1960).
4. "Spin Glasses: Irreversibility, Metalstability and the Free Energy Surface," G.S. Crest, C.M. Soukoulis, and K. Levin in Magnetic Phase Transitions; Springer-Verlag Berlin Heidelberg, 1983.
5. A. Brenner, D.E. Couch and E.K. Williams, J. Res. Natl. Bur. Stand 44, 109 (1950).
6. Paul A. Fleury, Science, Vol. 211, 125 (1981).
7. Kittel and Kroemer, Thermal Physics.
8. Intro. to Phase Transitions and Critical Phenomena by Eugene Stanley, Oxford University Press, London (1971).
9. K. Binder, J. de Phys. (Paris) 39, C6-1527 (1978).
10. D. Sherrington and S. Kirkpatrick, Phys. Rev. Lett. 35, 1792 (1975); Phys. Rev. B17, 4348 (1978).
11. S.F. Edwards and P.W. Anderson, J. Phys. F5, 965 (1975).
12. W. Abdul Razzaq and J.S. Kouvel, J. Appl. Phys. 55(6), 1623 (1984).
13. Manheimer, Bhagat, Chen; Phys. Rev. B26(1), 456 (1982).
14. Y. Yeshurun, M.B. Salamon, K.V. Rao and H.S. Chen, Phys. Rev. B24, 1536 (1981).
15. S. Senoussi, Phys. Rev. B31(9), 6086 (1985).
16. Dublon, Yeshurun, Phys. Rev. B25(7), 4899 (1982).
17. M.J. O'Shea and D.J. Sellmyer, J. Appl. Phys. 57(1), 3470 (1985).

18. M.J. O'Shea and D.J. Sellmyer, Phys. Rev. (to be published in 1985).

19. Handbook of Chemistry and Physics.

20. Intro. to Solid State Physics, Kittel.

21. M.A. Ruderman and C. Kittel, Phys. Rev. 96(1) 99 (1954).

22. Tadao Kasuya, Progress of Theoretical Physics, 16(1), 45 (1956).

23. Kei Yosida, Phys. Rev. 106(5), 893 (1957).

24. K.H.J. Buschow, J. Appl. Phys. 52(5), 3319 (1981).

25. K. Handrich, Phys. Stat. Solidi 32, K55 (1969).

26. S. Kobe, Phys. Status Solidi 41, K13 (1970).

27. S. Kobe and K. Handrich, Sov. Phys. Solid State 13, 734 (1971).

28. K.H.J. Buschow, J. Appl Phys. 53, 7713 (1982).

29. A. Fert and P.M. Levy, Phys. Rev. Letts. 44, 1538 (1980).

30. S.J. Poon and J. Durand, Phys. Rev. B16, 316 (1977).

31. J. Durand, R. Raj, S.J. Poon and J.I. Budrick, IEEE Trans,. Magn. MAG 14, 722 (1978).

32. R.W. Cochrane, R. Harris and M. Plischke, J. Non Crys. Solids, 15, 239 (1974).

33. K.H.J. Buschow, Rep. Prog. Phys. 40, 1179 (1980).

34. T. Mizoguchi and K. Yamauchi, J. Phys. (Paris) 35 Suppl. 5, C4-287 (1974).

35. L.J. Schowalter, M.B. Salamon, C.C. Tsuei, and R.A. Craven, Solid State Commun. 24, 525 (1977).

36. E. Fugueroa, L. Lundgren, O. Beckman, and S.M. Bhagat, Solid State Commun. 20, 961 (1976).

37. P. Gaunt, S.C. Ho, Gwyn Williams, and R.W. Cochrane, Phys. Rev. B23(1), 251 (1981).

38. K. Yamada, Y. Ishikawa, Y. Endoh and T. Masumoto, Solid State Commun. 16, 1335 (1975).

39. R. Malmhäll, G. Bäkström, K.V. Rao, S.M. Bhagat, M. Mejchle, and M.B. Salamon, J. Appl. Phys. 49, 1727 (1978).

40. S.N. Kaul and M. Rosenberg, Solid State Commun. 41(11), 857 (1982).

41. Y. Yeshurun, M.B. Salamon, K.V. Rao and H.S. Chen, Phys. Rev. Lett. 45, 1366 (1980); Solid State Commun. 38, 371 (1981).

42. L.S. Barton and M.B. Salamon, Phys. Rev. B25(3), 2030 (1982).

43. B.L. Yu, J.M.D. Coey, M. Olivier, and J.O. Ström-Olsen, J. Appl. Phys. 55 (1984).

MAGNETIC PHASE TRANSITIONS IN Gd-RICH METALLIC GLASSES

by

JAAFAR JANTAN

B.Sc., Kansas State University, 1983

AN ABSTRACT OF A MASTER'S THESIS

submitted in partial fulfillment of the requirements of the degree

MASTER OF SCIENCE

Department of Physics

Kansas State University

Manhattan, Kansas

1985

Abstract

The magnetic properties of amorphous $Gd_xTM_{72-x}G_{28}$ where TM = Mn, Ni and La and $G_{28} = Ga_{18}B_{10}$ were investigated using ac susceptibility and dc magnetization techniques in the temperature range 4.2K to 300K. Double transition behavior is present in all three systems studied. The multicritical point of the Gd-La and Gd-Mn systems are at about 67 at.% Gd and 38 at.% Gd respectively. Double transition behavior is present in all the compositions studied in the Gd-Ni system. The spin glass state in these systems exhibits non-equilibrium behavior. The magnetic isotherms around both the paramagnetic-ferromagnetic and ferromagnetic-spin glass transitions scale according to the static scaling hypothesis. Magnetic phase diagrams for all three systems are obtained from the transition temperatures determined from scaling.